

Effect of Annular Shape on Leaflet Curvature in Reducing Mitral Leaflet Stress

Ivan S. Salgo, MS, MD; Joseph H. Gorman III, MD; Robert C. Gorman, MD; Benjamin M. Jackson, MD; Frank W. Bowen, MD; Theodore Plappert, CVT; Martin G. St John Sutton, MBBS, FRCP; L. Henry Edmunds, Jr, MD

Background—Leaflet curvature is known to reduce mechanical stress. There are 2 major components that contribute to this curvature. Leaflet billowing introduces the most obvious form of leaflet curvature. The saddle shape of the mitral annulus imparts a more subtle form of leaflet curvature. This study explores the relative contributions of leaflet billowing and annular shape on leaflet curvature and stress distribution.

Methods and Results—Both numerical simulation and experimental data were used. The simulation consisted of an array of numerically generated mitral annular phantoms encompassing flat to markedly saddle-shaped annular heights. Highest peak leaflet stresses occurred for the flat annulus. As saddle height increased, peak stresses decreased. The minimum peak leaflet stress occurred at an annular height to commissural width ratio of 15% to 25%. The second phase involved data acquisition for the annulus from 3 humans by 3D echocardiography, 3 sheep by sonomicrometry array localization, 2 sheep by 3D echocardiography, and 2 baboons by 3D echocardiography. All 3 species imaged had annuli of a similar shape, with an annular height to commissural width ratio of 10% to 15%.

Conclusion—The saddle shape of the mitral annulus confers a mechanical advantage to the leaflets by adding curvature. This may be valuable when leaflet curvature becomes reduced due to diminished leaflet billowing caused by annular dilatation. The fact that the saddle shape is conserved across mammalian species provides indirect evidence of the advantages it confers. This analysis of mitral annular contour may prove applicable in developing the next generation of mitral annular prostheses. (*Circulation*. 2002;106:711-717.)

Key Words: finite element analysis ■ echocardiography ■ ultrasonics ■ valves

The shape of the mitral annulus conforms to a saddle configuration.¹⁻⁵ Sonomicrometry array localization, marker angiography, and 3D echocardiography confirm both the saddle shape and dynamic changes in mitral annular geometry during the cardiac cycle.^{1,6-9} However, a teleologic reason for nature's selection of this shape has not been proposed quantitatively. The effects of leaflet curvature on stress reduction have been described and are generally accepted as an important mechanism in the efficiency of valve function.¹⁰ Until now, the only component of leaflet curvature analyzed has been leaflet billowing. The contribution of annular shape on leaflet curvature and stress has not been described. The present study tests the hypothesis that the annular saddle shape imposes another form of leaflet curvature, which acts independently although synergistically with leaflet billowing to minimize leaflet stress.

Methods

Overview

The methods consist of a numerical simulation and experimental measurements. The first phase of the numerical simulation is

designed to isolate the relative contributions of leaflet billowing versus annular nonplanarity on leaflet stress reduction in a basic model. The next numerical phase is to study the synergistic effect of these 2 shape factors together in further reducing peak leaflet stress in an anatomically realistic design. Finally, the degree of annular nonplanarity predicted to minimize peak leaflet stress by the numerical simulation is compared with experimental data.

Numerical Simulation (Phase 1): Isolating the Effect of Leaflet Billowing Versus Annular Nonplanarity in Peak Stress Reduction

Two fundamental shapes (not leaflet designs) are generated: an elliptic paraboloid to model leaflet billowing with a flat annulus and a hyperbolic paraboloid to model annular nonplanarity with minimal leaflet billowing. These shapes are shown in Figure 1. The paraboloid with flat annulus (billowing leaflet model) is generated according to the following parametric formula in cylindrical coordinates:

$$(1) \quad ar \cos \theta, br \sin \theta, -h_b r^2$$

The "pure" saddle phantom (nonplanar annulus model) is generated according to the following formula:

$$(2) \quad ar \cos \theta, br \sin \theta, h_a r^2 \cos 2\theta$$

Received January 10, 2002; revision received May 23, 2002; accepted May 24, 2002.

From Philips Medical Systems (I.S.S.), Andover, Mass, and the Departments of Surgery (J.H.G., R.C.G., B.M.J., F.W.B., L.H.E.), Medicine (T.P., M.G.S.J.S.), and Anesthesia (I.S.S.), School of Medicine, University of Pennsylvania, Philadelphia, Pa.

Dr Salgo is an employee of Philips Medical Systems.

Presented in part at the 73rd Scientific Sessions of the American Heart Association, New Orleans, La, November 12-15, 2000, and published in abstract form (*Circulation*. 2000;102(suppl II):II-631).

Correspondence to Ivan S. Salgo, MS, MD, 500 Brookside Drive, Andover, MA 01810. E-mail ivan_salgo@attbi.com

© 2002 American Heart Association, Inc.

Circulation is available at <http://www.circulationaha.org>

DOI: 10.1161/01.CIR.0000025426.39426.83

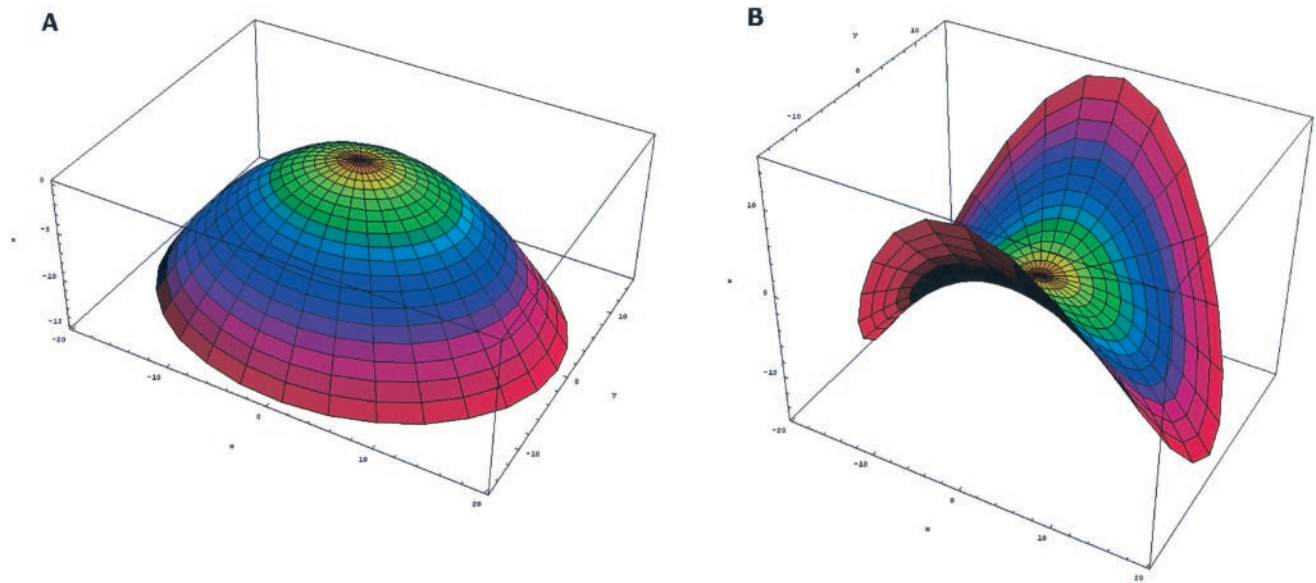


Figure 1. Plot of an elliptic (A) and hyperbolic (B) paraboloid as fundamental shapes, not leaflets. The annular dimensions are 38.75 mm across the major axis and 30 mm on the minor axis. The height is 15 mm, which corresponds to a dome-height ratio of 39% ($h_b/2a$) for A (billowing leaflet model) and an AHCWR of 39% (h_a/a) for B (nonplanar annulus model). The hue of the shapes varies by curvature using differential geometry. The configuration in B represents minimal surface area.

In both formulas, The length $2a$ represents the commissural diameter, $2b$ is the posterior-anterior diameter, and r is radius. Therefore, these parameters a and b control transverse annular dimension and hence flow area. The parametric equations 1 and 2 describe both an annulus and a surface. The parameter h_b controls dome height (degree of bulging) for the billowing leaflet model (equation 1), whereas annular half-height is controlled by h_a for the nonplanar annulus model (equation 2). To allow a comparison of theoretical results with experimental findings, 2 normalized parameters are defined. For the billowing leaflet model, normalized leaflet bulge (or billow) is defined as $h_b/2a$. For the nonplanar annulus model, the annular height to commissural width ratio (AHCWR) is computed as h_a/a . Using dimensions from published anatomic drawings, the parameter a is set at 19.4 mm and b at 15 mm.¹¹ The values h_b and $2h_a$, respectively, varied from 0 mm (a flat annulus and leaflets) to 38.75 mm, which corresponded to a dome height (billowing leaflet model) and AHCWR (nonplanar annulus model) of 100%. Using custom utilities and scripts written in C++ and Mathematica 4.0 (Wolfram Research), surfaces are plotted to discrete points and transferred to a commercial mesh generator and finite element solver (described below).

Numerical Simulation (Phase 2): Quantifying the Synergistic Effect of Leaflet Billowing and Annular Nonplanarity in Peak Stress Reduction in an Anatomically More Pragmatic Model

Two families of mitral phantoms are generated. Both families of leaflet design have constant flow orifice areas, but their annular height varies from 0 to 9.6875 mm or an AHCWR of 0% to 25%. The 2 families are distinct on the basis of the curvature of their leaflets: one has anterior and posterior leaflets of lesser curvature, whereas the other family has leaflets with more pronounced curvature as defined below. The mitral annular saddle is defined by the following parametric equation:

$$(3) \quad a \cos \theta, b \sin \theta, h_a \cos 2\theta$$

Equation 3 represents an annulus without leaflets because the variable r is removed. It defines a 3D space curve (ie, one wire frame), not a surface. Figure 2A displays a typical annular curve generated by the equation. For all phantoms, the parameter a is set to 19.4 mm and b to 15 mm. Therefore, the commissural diameter is

38.75 mm. The parameter h_a is varied to yield AHCWRs of 0%, 3%, 7%, 15%, 20%, and 25%. Two families of wire frames are constructed and transferred to a computer-aided design application (Superdraw and Supersurf, Algor, Inc). For each wire frame, a connecting line denoting the apposition of the anterior and posterior leaflets is interposed into the flat and saddle-shaped annuli as shown in Figure 2A. The center of this apposition line is connected to the aortic portion of the anterior annulus by either a curved or flat line in 3D space. Moreover, another line is connected to the midpoint of the posterior leaflet (centered within the potential medial scallop). For the flat family of phantoms, these are straight lines. For the leaflets with curved domes, they are circular arcs with tangential angles fixed at 35 and 70 degrees. Therefore, all leaflet phantoms have known curvature as described by computer-aided design techniques. Finally, the leaflets themselves are placed onto the phantom wire frames with nonuniform rational B-spline surfaces. These surfaces and general anatomic orientations are shown in Figure 2. There are 6 phantoms in each of the 2 families.

Finite Element Analysis of Mechanical Stress

Given a specific fundamental shape (Phase I) or mitral phantom (Phase II), the next step in the analysis is to solve the differential equations of continuum mechanics to compute leaflet stress. A commercial finite element solver was used to compute stresses (Algor, Inc). A specific material model and property is used for all shapes. This is a linear, static, orthotropic material model chosen to simulate the effect of predominant collagen orientation within the leaflets.^{12,13} The major material axis is oriented with respect to the commissure-to-commissure orientation. Table 1 shows the values used for the analysis. Leaflet thickness is kept constant over the entire valve and to simulate end systole, a peak pressure of 16 kPa (120 torr) is used for all calculations. Therefore, the computed leaflet stresses are derived from data designed to simulate peak load. The leaflets are bound to the annulus and chordal attachments by fixed boundary conditions because the leaflets themselves flex and do not have joints. Moreover, no attempt is made to simulate chordal structures. The leaflet models are first refined using a mesh generator to space the finite element nodes optimally. Orthotropic plate elements in 3D are set for the phantoms. Peak leaflet stresses using von Mises maximum distortion energy criterion are then collected from the analysis.^{14,15}

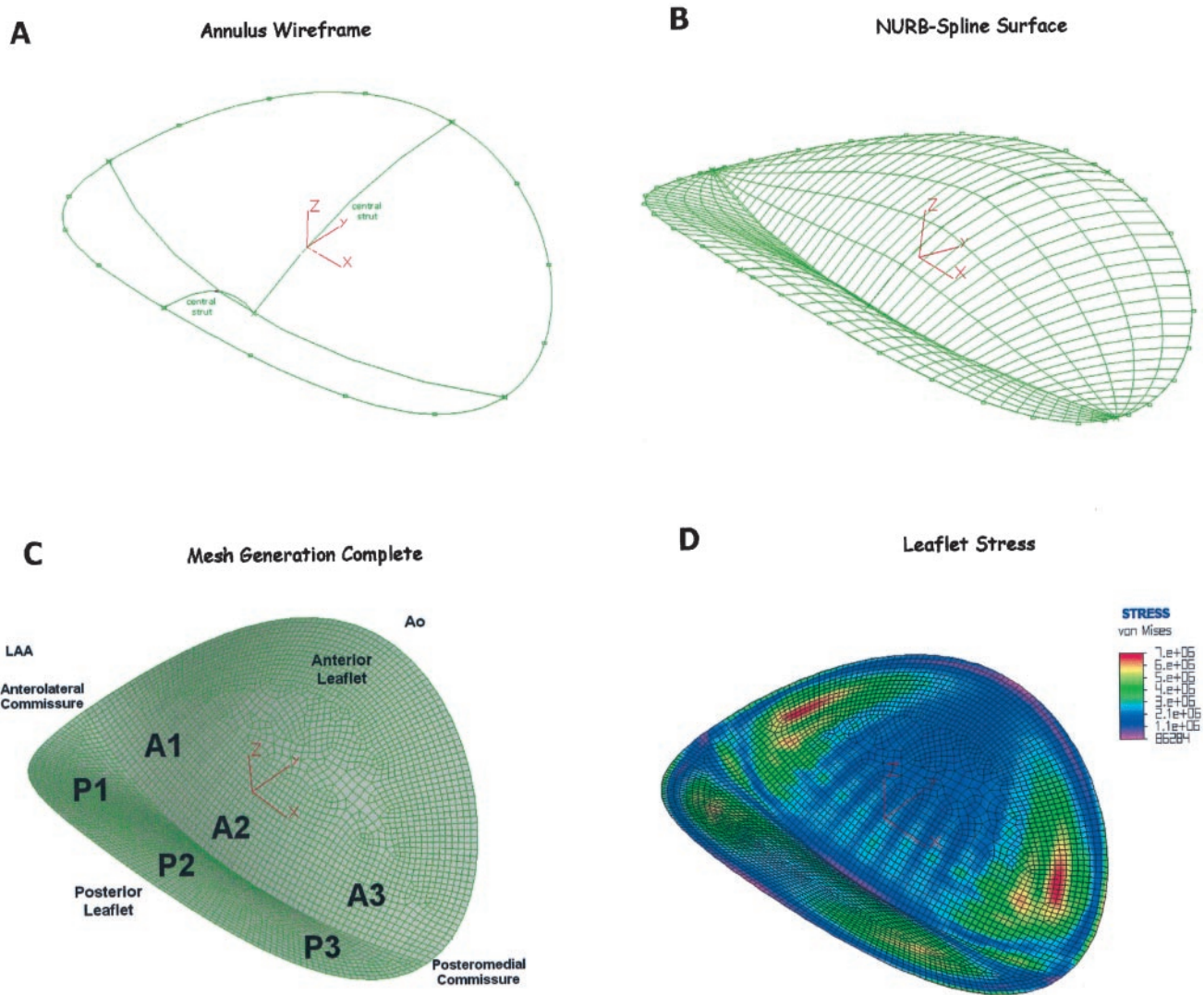


Figure 2. A, Figure of wire frame used to construct the mitral annulus and leaflets. The AHCWR was 20% for this case. The annulus shown here is saddle-shaped. The apposition of the anterior and posterior leaflet is shown across the major axis of the annulus. The central struts of the anterior and posterior leaflets are shown. These were either curved for domed leaflets or flat for flattened leaflets. B, Demonstration of nonuniform rational B-spline surfaces used to fit phantom leaflets. Collagen orientation is not shown. C, Model of phantom after mesh generation for optimal alignment of computational elements. Anatomic landmarks are labeled (LAA indicates location of left atrial appendage; Ao, aorta; A, anterior leaflet; P, posterior leaflet; and 1, 2, and 3, lateral, middle, and medial areas of the leaflets). The mesh shown was used numerically for the finite element solutions. D, Stress plot of linear static analysis.

Human Imaging Protocol

After approval from the Institutional Review Board, 3 people were scanned using 5 to 6.2 MHz multiplane transesophageal echocardiography (Omniplane II, Philips Medical Systems). Only subjects scheduled for first-time coronary revascularization and transesophageal echocardiography who gave consent were selected. The anesthetic included narcotic and inhalational agents (fentanyl 20 to 40 $\mu\text{g}/\text{kg}$ and isoflurane 1% vol). All patients had normal ejection fractions and ventricular size. Data acquisition was gated to the ECG and respiration. Images were then centered about the mitral annulus and obtained every 10 degrees at end-systole and stored onto a magneto-optical disk for offline analysis. Images were gated to end-systole for all studies.

Ovine Surgical and Echocardiographic Imaging Protocol

Two Dorsett hybrid sheep (40 to 50 kg) were given sodium thiopental (7 mg/kg IV), intubated, anesthetized with isoflurane

(1.5% to 2%), and ventilated with oxygen (Narkomed, North American Drager). All animals received glycopyrrolate (0.01 to 0.02 mg/kg IV), cefazolin (1 g IV) and gentamicin (80 mg IV). A thoracotomy incision was performed, and the heart was supported in a pericardial cradle. Three-dimensional echocardiographic scanning was performed at the cardiac apex, and 3D data were acquired every 5 degrees using a handheld 5 MHz rotational probe (Transthoracic Omniplane, Philips Medical Systems) and stored onto a magneto-optical disk. Images were gated to end-systole for all studies. Sheep were treated in compliance with NIH publication No. 85-23 as revised in 1985.

Sonomicrometry Array Localization

Three separate sheep underwent general anesthesia as described above and were placed on cardiopulmonary bypass. Through a left atriotomy, 12 sonomicrometry transducers were placed equidistant around the annulus. The animals were weaned from bypass, the incision was closed, and the animals were allowed to recover. Seven days later, intratransducer distance measurements were taken every 5

TABLE 1. Material Properties Used for Finite Element Analysis Loaded at Peak Systole

Thickness, mm	1.31
Young's modulus, major axis (E_x), kPa	6230.0
Young's modulus, minor axis (E_y), kPa	2350.0
Poisson's ratio, major axis, ν_1	0.45
Poisson's ratio, minor axis, ν_2	0.17
Bulk modulus, G_{xy}	1370.0
Peak systolic pressure, P (torr)	120.0

This material represents a composite type with increased stiffness across one dimension over its orthogonal dimension. This represents a predominance of the orientation of collagen within the leaflet. Most of these data were derived experimentally and are reported in the literature.

ms throughout the cardiac cycle. The 3D coordinates of each transducer were then derived from the distance data using a multi-dimensional scaling technique.

Baboon Echocardiographic Imaging Protocol

Two adult baboons (13 and 18 kg) were given ketamine (10 mg/kg IV), intubated, anesthetized with isoflurane (1.5% to 2%), and ventilated with oxygen (Narkomed, North American Drager). All animals received atropine (0.01 to 0.02 mg/kg IV), cefazolin (1 g IV), and gentamicin (80 mg IV). Baboons were treated in compliance with NIH publication No. 85-23 as revised in 1985.

The baboons were imaged from the chest wall by 3D multiplane echocardiography. Data were acquired from 2 baboons every 5 degrees using a handheld rotational probe (Transthoracic Omniplane) and stored onto a magneto-optical disk for offline analysis. Images were gated to end-systole for all studies.

3D Echo Image Analysis

Using custom image manipulation software written for this work, the mitral annulus was identified offline from the 3D echocardiographic studies. Annular points (2 for each corresponding angle from the representative image) were transformed in 3D space. These points were calibrated to the depth setting of the imaging probe, and the aspect ratio was accounted for by a constant in the software. The mitral annulus was fit to a plane using the following formula:

$$(4) \quad \frac{x}{a} + \frac{y}{b} + \frac{z}{c} = 1$$

Its orientation minimizes the least squares error. The xy plane is oriented orthogonal to flow. Using a quaternion geometric transformation, the maximum and minimum annular heights (z axis) are compared with the maximum cross-sectional diameter. Data acquired from echocardiography or sonomicrometry are interpolated and analyzed using a discrete Fourier transform with a Gaussian convolution kernel. This is used for both visualization and quantitation. Figure 3 demonstrates one of the echocardiographic reconstructions done on a human subject. The AHCWR was computed for the 3 humans, 5 sheep, and 2 baboons.



Figure 3. Fourier smoothed mitral annulus reconstruction from a human subject. The data used to acquire this image was gathered by transesophageal echocardiography. The commissures are located at the low points of the saddle.

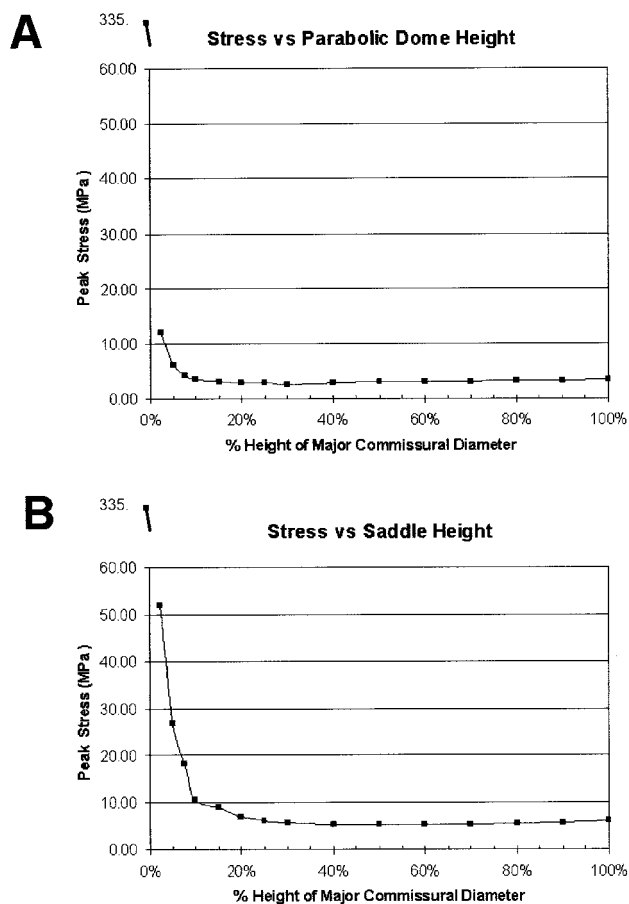


Figure 4. Plot of peak stress versus percent height. The elliptic paraboloid (A) and the hyperbolic paraboloid (B; saddle) are shown. A, Peak stress for the billowing leaflet model. B, Peak stress for the nonplanar annulus model. A flat disc results when the parameters for each model, h_b and h_a respectively, are set to 0. The peak stress of the flat disc is 335 MPa in A and B.

Results

Phase I: Finite Element Analysis of the Effect of Leaflet Billowing Versus Annular Nonplanarity in Peak Stress Reduction

Peak stresses are affected by intrinsic shape changes for a constant flow orifice area. The peak stress for a flat disc is 335 MPa (where 1 Pascal=1 Newton/m²=10 dyne/cm²). Figure 4A demonstrates that leaflet billowing reduces peak leaflet stress relative to the flat annulus. Small changes in the shape of the leaflet (ie, the introduction of leaflet curvature) result in marked reductions of peak leaflet stresses. Even for a normalized height of 3%, leaflet stress is reduced 28-fold. An approximate minimum occurs at a normalized height of 30%. However, there is no substantial reduction between 10% and 40%. Figure 4B demonstrates that the fundamental saddle shape has a significantly lower peak leaflet stress than the flat disc. As the AHCWR increases away from zero, peak stresses in the leaflets diminish. There is a 37-fold reduction in peak leaflet stress at an AHCWR of 20%. Reductions in peak stress reach a minimum at 25% AHCWR and higher. The plate model indicates that peak stresses increase for both shapes after inordinate increases in normalized dome height or an AHCWR >60% (Figure 4).

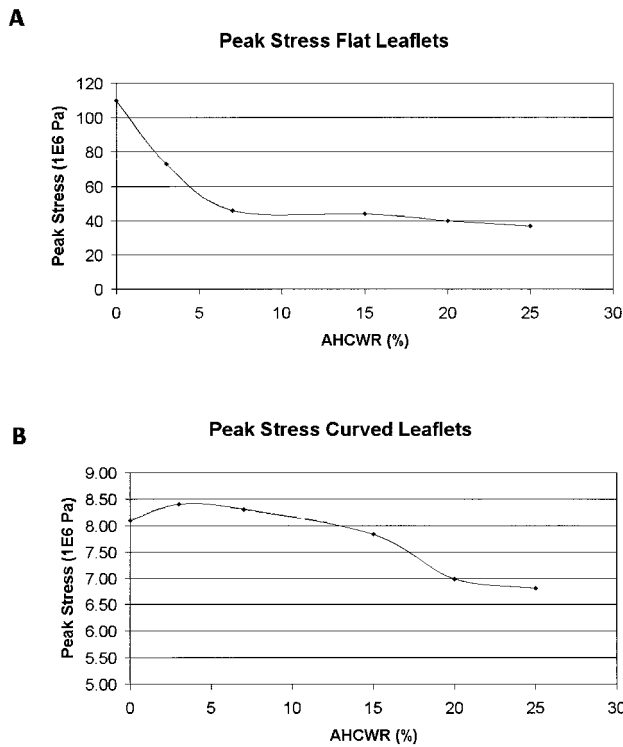


Figure 5. Plot of peak leaflet stress (A, flat leaflets; B, curved leaflets) versus AHCWR for the mitral phantoms (phase II) described in this article.

Phase 2: Finite Element Analysis of the Synergistic Effect of Leaflet Bulging and Annular Nonplanarity in Peak Stress Reduction

Figure 5 shows peak stresses for the mitral phantoms. Because the center of the leaflet is supported by chordal boundaries, peak leaflet stress is lower than that of the flat annulus presented in the prior section: 110 MPa (Figure 5A) versus 336 MPa (Figure 4), respectively. Figure 5 shows that for both families of mitral phantoms (flattened and curved leaflets), introduction of the saddle-shaped annulus reduces peak leaflet stress. Increasing AHCWR to 20% with flat leaflets reduces peak leaflet stress 3-fold from 110 MPa to

TABLE 2. Results of 3D Transesophageal Echocardiography and Transthoracic Omniplane Echocardiography for 3 Humans, 2 Sheep, and 2 Baboons

Subject	Acquisition	AHCWR
Subject 1	3D TEE	16
Subject 2	3D TEE	14
Subject 3	3D TEE	14
Sheep 1	SAL	13
Sheep 2	SAL	19
Sheep 3	SAL	7
Sheep 4	3D TTO	17
Sheep 5	3D TTO	12
Baboon 1	3D TTO	14
Baboon 2	3D TTO	17

Results of 3 sheep using sonomicrometry array localization (SAL) are also presented. AHCWR is shown as a percentage. TEE indicates transesophageal echocardiography; TTO, transthoracic omniplane echocardiography.

<40 MPa. The addition of curved leaflets (bulging) to the 20% AHCWR model decreases the total leaflet stress another 5-fold to 7 MPa. Figure 6 shows stress distribution for a valve with an AHCWR of 20%. Figures 5 and 6 illustrate the synergistic nature of combined leaflet bulging and the annular saddle shape on peak mitral valve leaflet stress. With or without leaflet billowing, the stress reduction associated with annular saddle shape reaches a maximum effect at an AHCWR value between 15% and 20% (Figure 5).

Experimental Determination of Mitral Annular Height

Table 2 displays the annular height ratios found in 3 species. All have a saddle-shaped mitral annuli. Three-dimensional echocardiographic determinations of the 3 human patients yield an AHCWR of 14% to 16%. The 2 sheep studied by echocardiography have AHCWRs of 12% and 17%. Sonomicrometry results yield AHCWRs of 13%, 19%, and 7% for different sheep. Finally, the 2 baboons have AHCWRs of 14% and 17%.

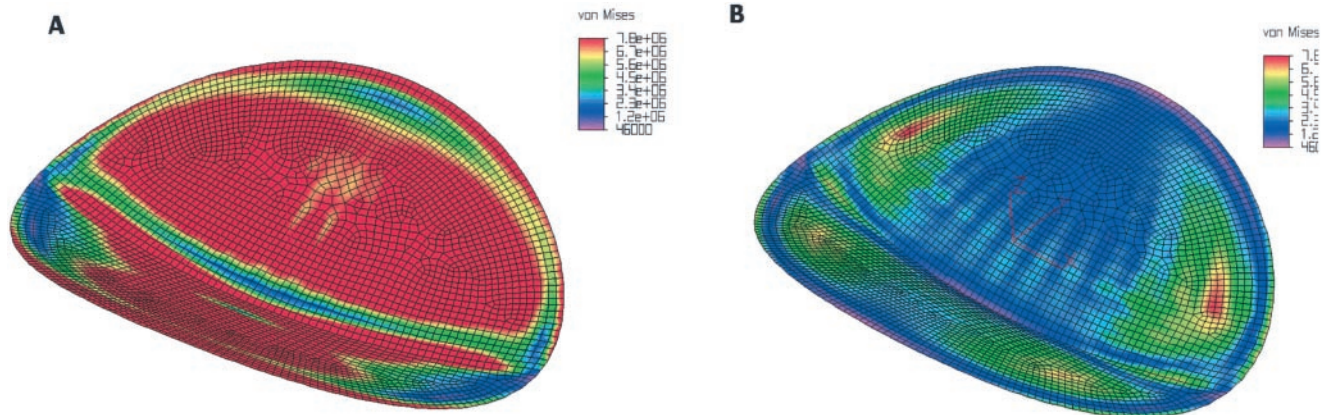


Figure 6. A, Plot of mitral phantom leaflets without billowing showing stresses by von Mises distortion energy theory. B, Plot of mitral phantom leaflet with billowing showing stresses by von Mises distortion energy theory. The AHCWR was 15% for both cases. Note the decrease in stress for the curved leaflets in B.

Discussion

This study corroborates the conclusion that leaflet billowing reduces peak leaflet stress considerably.¹⁰ It also supports the hypothesis that mitral annular nonplanarity further reduces peak leaflet stress. The synergistic combination of leaflet billowing and annular nonplanarity act together to optimize leaflet curvature, thereby minimizing peak mitral leaflet stress. These results, coupled with general principles of mechanics, show that mitral leaflet stress is determined by load (the pressure differential between the left ventricle and atrium), leaflet area, and leaflet curvature.^{16–19}

Finite element analysis is a tool used to solve the differential equations of mechanical stress. This computer-based technique is used to solve problems of arbitrarily defined geometry according to a specific design because only the most simple of shapes can be solved analytically by hand. For example, linear static finite element computer modeling of the mitral valve has been used to examine general mechanical properties. For static linear models, computation of stress (although not strain) yields the same final result independent of material modulus.

The simulation for phase II was designed to extend the hypothesis to a more realistic geometric shape, one that specifically uses chordal support. An early study using a Laplace's law model indicated that curvature of the leaflets is beneficial. For the current study, the leaflets were designed to satisfy the following design constraints. First, symmetry of leaflets was preserved with reference to the commissures. This assumes that peak stresses of equal magnitude occur bilaterally. Second, the posterior leaflets were not scalloped (ie, sharply marginalized) to study the effect of the annulus on leaflets that may lose curvature *in vivo*. The design, although more realistic than the first part, is intentionally kept constrained to understand effects of stress by controlling perturbations of leaflet design. Under these conditions, the data for the mitral phantom simulation demonstrate that (1) leaflet curvature is a major determinant of leaflet stress and (2) the saddle shape of the annulus contributes to reductions in leaflet stress by providing another mechanism of leaflet curvature in addition to leaflet billowing.

Two different imaging techniques that were performed to verify these predictions show that the saddle shape of the mitral annulus is preserved across 3 mammalian species. All subjects had an AHCWR of $\approx 15\%$ (with one outlier), and none of the subject hearts was dilated. The finite element analyses consistently demonstrate that leaflet stress reductions occur in the range of AHCWRs of 15% to 20%. These data strongly suggest that nature conserves the saddle-shaped annulus for a mechanical benefit.

Analysis of actual leaflet shapes by imaging studies was not a goal of this study because of errors created by spatiotemporal shifting in gated 3D echocardiographic techniques.^{20–23} Medical imaging techniques are only beginning to acquire data (of the fidelity needed for this type of analysis) of structures that move as quickly as leaflets. Because the annulus has much slower velocity components than the leaflets during the cardiac cycle, gated 3D echocardiography was used to image the annulus. However, optimal annulus filtering techniques in the Fourier (spectral) domain are not

well established. Excessive low pass spatial filtering yields an annulus that is flatter than actual. Without spatial filtering, all AHCWRs would be higher, and thus our data report the lower bounds. This may explain why our experimental results tended toward the low end (15% AHCWR) of the predicted stress-minimizing AHCWR range of 15% to 20%. As real time magnetic resonance and matrix array 3D echocardiographic techniques evolve, imaging of the entire leaflets themselves with subsequent finite element analysis will become feasible. These results, taken in conjunction with the theoretical calculations presented above, provide compelling evidence that the saddle shape of the mitral annulus significantly reduces leaflet stress at AHCWR ratios between 15% to 20%.

The analysis presented in this study provides insight into potential methods for improving current mitral valve repair techniques. Over the past 20 years, Carpentier has pioneered and standardized surgical techniques that allow reliable repair of valves with leaflet, chordal, and annular deformities.²⁴ The widespread use of these techniques has produced notable results at centers all over the world. Although the durability of these repairs has been relatively impressive, there is a long-term failure rate of between 5% and 12% (return of significant mitral regurgitation) at 10 years, depending on the type of initial leaflet or annular pathology.^{25–27} Twenty year recurrence rates for repaired rheumatic valves may be as high as 50%.²⁸ In most cases, these long-term failures are the result of disruption at leaflet, chordal, or annular suture lines, suggesting mechanical stress as an etiological factor.²⁹

Most surgeons with experience in mitral valve repair agree that restoration of normal annular geometry with ring annuloplasty is an essential component to all mitral valve repairs. In fact, it has been shown that leaflet repairs without ring annuloplasty are less durable than those that include it.²⁶ All currently available annuloplasty rings are flat. When implanted, these devices only restore the annulus to a more normal size in 2 dimensions. The height of the annulus is totally flattened by these devices, potentially placing undue stress and subsequent strain on the leaflet and chordal suture lines of the repair by diminishing leaflet curvature. Moreover, using larger saddle-shaped annular prostheses instead of their flat counterparts could allow increases in flow area while keeping peak leaflet stresses reduced. With this understanding, it seems reasonable to hypothesize that a saddle-shaped annuloplasty ring may increase mitral valve repair durability by reducing leaflet and chordal strain.

Acknowledgments

Supported by a beginning Grant-in-Aid from the American Heart Association, Pennsylvania-Delaware Affiliate (to I.S.S.); grants HL63594 (to R.C.G.) and HL 36308 (to L.H.E.) from the National Heart, Lung, and Blood Institute of the National Institutes of Health; and a grant from the Mary L. Smith Charitable Trust, Philadelphia Pa. The authors gratefully thank Hubert Yeung and Michael Peszynski for a discussion of the finite element findings.

References

1. Flachskampf FA, Chandra S, Gaddipati A, et al. Analysis of shape and motion of the mitral annulus in subjects with and without cardiomyopathy by echocardiographic 3-dimensional reconstruction. *J Am Soc Echocardiogr*. 2000;13:277–287.

2. Gorman JH III, Gorman RC, Jackson BM, et al. Distortions of the mitral valve in acute ischemic mitral regurgitation. *Ann Thorac Surg.* 1997;64:1026–1031.
3. Gorman RC, McCaughan JS, Ratcliffe MB, et al. Pathogenesis of acute ischemic mitral regurgitation in three dimensions. *J Thorac Cardiovasc Surg.* 1995;109:684–693.
4. Komeda M, Glasson JR, Bolger AF, et al. Geometric determinants of ischemic mitral regurgitation. *Circulation.* 1997;96(suppl 9):II-128–II-133.
5. Levine RA, Handschumacher MD, Sanfilippo AJ, et al. Three-dimensional echocardiographic reconstruction of the mitral valve, with implications for the diagnosis of mitral valve prolapse. *Circulation.* 1989;80:589–598.
6. Applebaum RM, Kasliwal RR, Kanojia A, et al. Utility of three-dimensional echocardiography during balloon mitral valvuloplasty. *J Am Coll Cardiol.* 1998;32:1405–1409.
7. Chen Q, Nosir YF, Vletter WB, et al. Accurate assessment of mitral valve area in patients with mitral stenosis by three-dimensional echocardiography. *J Am Soc Echocardiogr.* 1997;10:133–140.
8. Gilon D, Cape EG, Handschumacher MD, et al. Insights from three-dimensional echocardiographic laser stereolithography: effect of leaflet funnel geometry on the coefficient of orifice contraction, pressure loss, and the Gorlin formula in mitral stenosis. *Circulation.* 1996;94:452–459.
9. Salgo IS. Three-dimensional echocardiography. *J Cardiothorac Vasc Anesth.* 1997;11:506–516.
10. Arts T, Meerbaum S, Reneman R, et al. Stresses in the closed mitral valve: a model study. *J Biomech.* 1983;16:539–547.
11. Netter F. *CIBA Collection of Medical Illustrations.* Teterboro, NJ: Icon Learning Systems; 1986.
12. Kunzelman KS, Cochran RP, Chuong C, et al. Finite element analysis of the mitral valve. *J Heart Valve Dis.* 1993;2:326–340.
13. Kunzelman KS, Cochran RP, Murphree SS, et al. Differential collagen distribution in the mitral valve and its influence on biomechanical behaviour. *J Heart Valve Dis.* 1993;2:236–244.
14. Bathe KJ. *Finite Element Procedures.* Upper Saddle River, NJ: Prentice-Hall; 1996.
15. Spyrakos CC, Raftoyiannis J. *Linear and Nonlinear Finite Element Analysis in Engineering Practice.* Pittsburgh, Pa: Algor, Inc; 1997.
16. el Asmar B, Acker M, Couetil JP, et al. Mitral valve repair in the extensively calcified mitral valve annulus. *Ann Thorac Surg.* 1991;52:66–69.
17. Yamaura Y, Yoshikawa J, Yoshida K, et al. Three-dimensional analysis of configuration and dynamics in patients with an annuloplasty ring by multiplane transesophageal echocardiography: comparison between flexible and rigid annuloplasty rings. *J Heart Valve Dis.* 1995;4:618–622.
18. Yamaura Y, Yoshida K, Hozumi T, et al. Three-dimensional echocardiographic evaluation of configuration and dynamics of the mitral annulus in patients fitted with an annuloplasty ring. *J Heart Valve Dis.* 1997;6:43–47.
19. Balasundaram SG, Duran C. Surgical approaches to the mitral valve. *J Card Surg.* 1990;5:163–169.
20. Gopal AS, Schnellbaecher MJ, Shen Z, et al. Freehand three-dimensional echocardiography for measurement of left ventricular mass: in vivo anatomic validation using explanted human hearts. *J Am Coll Cardiol.* 1997;30:802–810.
21. King DL, Gopal AS, Keller AM, et al. Three-dimensional echocardiography: advances for measurement of ventricular volume and mass. *Hyper-tension.* 1994;23:1172–1179.
22. Legget ME, Leotta DF, Bolson EL, et al. System for quantitative three-dimensional echocardiography of the left ventricle based on a magnetic-field position and orientation sensing system. *IEEE Trans Biomed Eng.* 1998;45:494–504.
23. Salustri A, Becker AE, van Herwerden L, et al. Three-dimensional echocardiography of normal and pathologic mitral valve: a comparison with two-dimensional transesophageal echocardiography. *J Am Coll Cardiol.* 1996;27:1502–1510.
24. Carpentier A. Cardiac valve surgery: the “French correction.” *J Thorac Cardiovasc Surg.* 1983;86:323–337.
25. Braunberger E, Deloche A, Berrebi A, et al. Very long-term results (more than 20 years) of valve repair with Carpentier’s techniques in non-rheumatic mitral valve insufficiency. *Circulation.* 2001;104(12 Suppl 1):I-8–I-11.
26. Cohn LH, Couper GS, Aranki SF, et al. Long-term results of mitral valve reconstruction for regurgitation of the myxomatous mitral valve. *J Thorac Cardiovasc Surg.* 1994;107:143–150.
27. David TE, Armstrong S, Sun Z, et al. Late results of mitral valve repair for mitral regurgitation due to degenerative disease. *Ann Thorac Surg.* 1993;56:7–12.
28. Chauvaud S, Fuzellier JF, Berrebi A, et al. Long-term (29 years) results of reconstructive surgery in rheumatic mitral valve insufficiency. *Circulation.* 2001;104(12 Suppl 1):I-12–I-15.
29. Gillinov AM, Cosgrove DM, Blackstone EH, et al. Durability of mitral valve repair for degenerative disease. *J Thorac Cardiovasc Surg.* 1998;116:734–743.